Journal of ELECTRONIC MATERIALS, Vol. 49, No. 6, 2020
https://doi.org/10.1007/s11664-020-08102-0

Effect of Ag Content on Photocatalytic Activity of Ag@TiO_2/rGO Hybrid Photocatalysts

EYYUP CAN DOLUEL,[1,2] UGUR KARTAL,[2] TUNCAY DIKICI,[3] and METIN YURDDASKAL[4,5]

1.—Department of Metallurgical and Materials Engineering, Kocaeli University, Kocaeli, Turkey. 2.—The Graduate School of Natural and Sciences, Dokuz Eylul University, Izmir, Turkey. 3.—Torbali Vocational School, Dokuz Eylul University, Izmir, Turkey. 4.—Department of Metallurgical and Materials Engineering, Dokuz Eylul University, Izmir, Turkey. 5.—e-mail: metin.yurddaskal@deu.edu.tr

In this study, silver (Ag)-doped titanium dioxide/reduced graphene oxide (Ag@TiO_2/rGO, TGA) hybrid photocatalysts were synthesized for enhanced photocatalytic properties. TGA hybrid photocatalysts were synthesized through a facile sol–gel method. Synthesis of graphene oxide (GO) nanoparticles were obtained by Hummer's method followed by chemical reduction to obtain rGO nanoparticles. Ag doping was carried out at the sol stage of the sol–gel synthesis. Increasing amounts of Ag nanoparticles from 0.5 wt.% to 4 wt.% were added to increase the degradation effect of methylene blue (MB) under UV light irradiation. X-ray diffractometry (XRD), scanning electron microscopy (SEM), x-ray photoelectron spectroscopy (XPS), UV-vis spectrophotometry, photoluminescence spectroscopy (PL), and diffuse reflectance spectroscopy (DRS) were used to investigate the crystal structure, topography, morphology, chemical and optical properties of the samples, respectively. Samples were calcined in order to obtain the anatase phase at 500°C with a heating rate of 10°C/min for 2 h in air atmosphere. The effect of Ag content on the photocatalytic properties of TiO_2 based nanocomposite material was observed by keeping the weight ratio of rGO constant at 4 wt.%. Ag addition into the TiO_2/rGO matrix exposed an excellent photocatalytic activity under UV light irradiation than that of undoped TiO_2/rGO photocatalyst. The absorbance value of MB was degraded from 0.683 to 0.011 at 664 nm by TGA1 sample for 240 min. This demonstrated that the TGA1 hybrid photocatalyst containing 1 wt.% of Ag exhibited the highest degradation efficiency of 98.4%. This paper indicates the potential photocatalytic application of Ag-doped TiO_2/rGO photocatalysts on the removal of dissolved organic pollutants in water.

Key words: TiO_2, reduced graphene oxide, hybrid photocatalyst, Ag doping, photocatalytic activity

INTRODUCTION

Titanium dioxide (TiO_2) has attracted a great deal of attention for its potential applications in catalysis,[1] dye-sensitized solar cells,[2] water splitting,[3] air purification,[4] optical sensors[5] and rechargeable lithium-ion batteries.[6] Among various semiconductors, TiO_2 has many advantages including high chemical stability, non-toxicity, low cost, excellent photocatalytic efficiency and ease of synthesis.[7,8] However, TiO_2 mainly absorbs in the ultraviolet (UV) region and has very limited absorption in the visible region due to its wide band gap (3.0–3.2 eV). Also, the rapid recombination of the photoinduced electron–hole pairs leads to a low photocatalytic performance.[9] Correspondingly, a variety of

(Received December 31, 2019; accepted March 19, 2020; published online April 2, 2020)

strategies have been employed to solve these problems, including doping with noble metals (Pt, Au, Ag, Pd, etc.)[10–12] and nonmetals (N, S, C, B, I, etc.),[13–16] dye sensitization,[17] semiconductor coupling (Ag_2O, WO_3, ZnO, CdS, SiC, etc.),[18,19] and layered semiconductors.[20]

During the last decade, carbonaceous materials, such as carbon nanotubes, fullerenes, activated carbon, graphene, carbon nanohorns, and carbon nanowalls, have been extensively studied for enhancing photocatalytic activities of metal oxide semiconductors.[21–28] Especially, the high electrical conductivity of graphene helps in transferring photo-reduced electrons from the conduction band of TiO_2 owing to its less negative redox potential than the conduction band edge of TiO_2.[29–32] Graphene is a two-dimensional (2D) single-atom-thick sheet of graphite (Gr), which has astounding properties such as unique electrical and thermal conductivities, high specific surface area and high charge carrier mobility.[33,34] Thus, graphene may increase photocatalytic activity for the following reasons: increases the adsorption ability due to its large specific surface area, helps in transferring photo-reduced electrons from the conduction band of TiO_2 owing to its less negative redox potential than the conduction band edge of TiO_2, increases light adsorption since it acts as a photosensitizer.[35–39] However, due to the hydrophobic layers of graphene, it is difficult to fabricate TiO_2-graphene composites in an aqueous medium. Therefore, graphene oxide can be obtained with an oxidation process which has more hydrophilic layers, thanks to functional groups (such as –OH and –COOH) that include oxygen but these functional groups decreases the charge mobility. By the reduction process, some functional groups leave the structure and thus reduced graphene oxide (rGO) can be obtained. As a result, rGO structure is more stable than GO and shows almost similar properties as graphene.[35, 40–43]

TiO_2, one of the most promising photocatalysts, has attracted considerable attention to absorb UV light. The energy of UV light is only 5% of the total spectrum of sunlight. Therefore, embedding noble metal particles on the TiO_2 structures could enhance photosensitivity, which spreads light absorption to the visible light zone and allows the usage of the sunlight spectrum.[10–12, 44] In addition, noble metal doping into the TiO_2 structure forms a Schottky barrier, which gains electron trapping ability. Thereby, electron–hole recombination can be blocked.[29, 45, 46]

To the best of our knowledge, there are very limited studies on the enhancement of photocatalytic activities of TiO_2 by rGO and silver (Ag). Herein, TGA hybrid photocatalyst materials were produced through a facile and reproducible sol–gel method. We have investigated the effects of Ag content in the rGO/TiO_2 composite on the photocatalytic degradation of methylene blue (MB) under UV light irradiation.

EXPERIMENTAL DETAILS

Materials

Titanium (IV) isopropoxide (TTIP, $C_{12}H_{28}O_4Ti$, 97%), hydrazine hydrate (N_2H_4, 100%), glacial acetic acid (CH_3CO_2H) and silver nitrate ($AgNO_3$, 99%) were supplied by Merck. Gr flakes were supplied by Selen Chemistry. Potassium permanganate ($KMnO_4$, 99%) was supplied by Edukim. Hydrogen peroxide (H_2O_2, 35%), sulphuric acid (H_2SO_4, 95–97%), absolute ethanol (C_2H_6O) and methylene blue ($C_{16}H_{18}ClN_3S$) were purchased from Merck. Hydrochloric acid (HCl, 30–32%) was supplied by Tekkim.

Synthesis of GO and rGO

The preparation of graphene oxide was carried out using a modified Hummer's method.[47] Gr flakes and H_2SO_4 were added into a beaker which was placed in an ice bath and the mixture was stirred by a magnetic stirrer at 600 rpm at 20°C for 30 min to produce a fine dispersion. $KMnO_4$ was added very slowly to this mixture, keeping the temperature below 20°C. The mixture was further stirred for 3 h. This solution was then diluted by distilled water added dropwise. After mixing for a certain period of time, 100 mL distilled water was added to terminate the reaction. Mixing continued until the color of the solution turned brown. The mixture was treated with H_2O_2 and stirred for 1 h. The solution was centrifuged and the synthesized mass was washed with HCl and distilled water (1:9) solution three times and was then dried in an oven at 100°C to obtain GO powder.

Graphene oxide was reduced by chemical reduction. A reflux setup prepared for reduction of GO. GO was put into a round bottom flask, and distilled water was then added. The solution was stirred to produce a homogeneous solution. N_2H_4 was used as the reducing agent in order to obtain rGO. It was added dropwise and the solution was maintained for 12 h at 80°C. The obtained GO was separated by centrifuging and washing with distilled water several times. After washing, the same drying procedure was applied. As a result of this process, rGO powder was obtained.

Synthesis of Ag-Doped TiO_2/rGO Hybrid Photocatalyst Powders

Specified weight ratios of $AgNO_3$ and 4 wt.% rGO powder were used with C_2H_6O in different beakers and sonicated in an ultrasonic bath for 1 h. The solutions were then mixed together and stirred for 30 min. TTIP precursor and CH_3CO_2H were added dropwise to this mixture to ensure the formation of TiO_2 in the structure of hybrid photocatalysts. The obtained solution was stirred at 60°C for 5 h. After

Table I. Contribution amounts and names of the composites

Name	T	TGA0	TGA05	TGA1	TGA2	TGA4
wt.% Ag	0	0	0.5	1	2	4
wt.% TiO_2	100	96	95.5	95	94	92
wt.% rGO	0	4	4	4	4	4

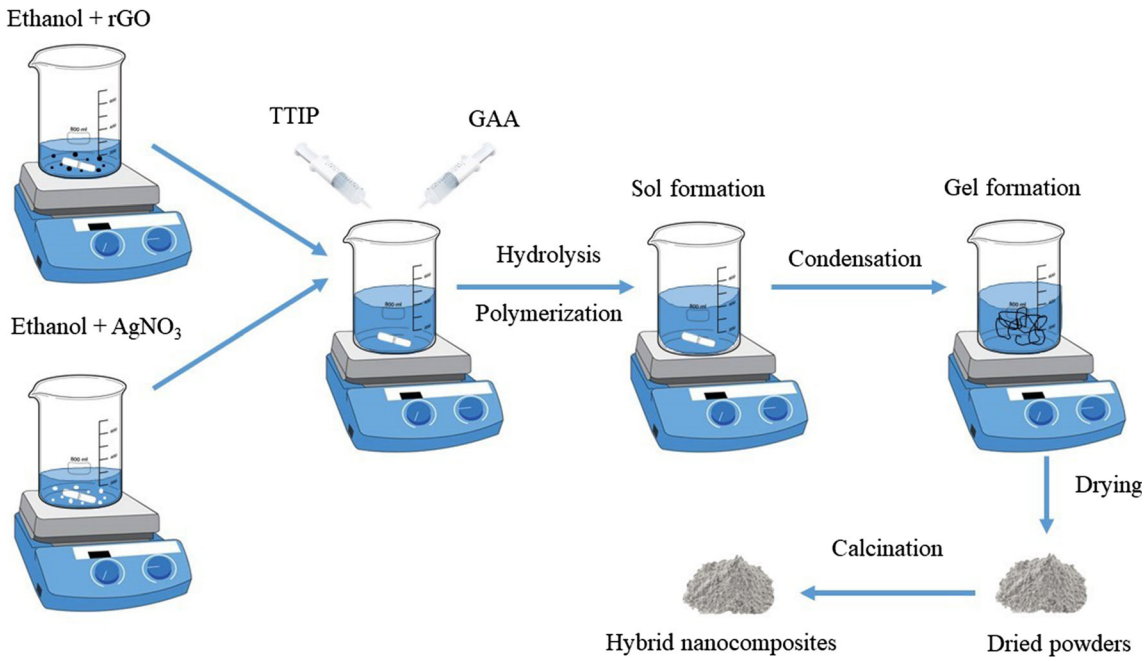

Fig 1. Schematic representation for the synthesis of TGA hybrid photocatalysts by sol–gel method.

mixing, the solution was dried completely at 150°C in an oven. The acquired powders were heat-treated at 500°C with a heating rate of 10°C/min for 2 h in order to enusre that the anatase phase had the most effective photocatalytic activity than the other TiO_2 phases (rutile, brookite).[48, 49]

It has been shown in our previous study[50] that the best photocatalytic efficiency was achieved with 4 wt.% rGO contribution. Therefore, in this study, the molar ratio of rGO was kept constant, and Ag content was investigated as having the potential to enhance the photocatalytic activity of TiO_2/rGO hybrid composites. All amounts of Ag, TiO_2 and rGO contributions are listed and named in Table I. All production steps of the Ag-doped rGO/TiO_2 hybrid photocatalysts are given in detail in Fig. 1.

Characterization

Scanning electron microscopy (SEM, Coxem EM-30 Plus) is used to investigate the microstructure of the hybrid photocatalysts. The phase structures of hybrid photocatalysts were identified by X-ray diffraction analysis (XRD, Thermo ARL X'TRA) with Ni-filtered Cu-K_α radiation (1.5418 Å) at a scan rate of 2°/min in the 2θ range of 3°–90°. Chemical analyses of the hybrid photocatalysts were characterized by X-ray photoelectron spectroscopy (XPS, Thermo Scientific). Optical properties of the hybrid photocatalysts were investigated with photoluminescence spectroscopy (PL, Edinburg Instruments FLSP920), and diffuse reflectance spectroscopy (DRS, Thermo Scientific Evolution 600).

Preparation of Photocatalytic Activity Measurement System

MB was selected for pollutant removal in order to observe the photocatalytic activity of TGA hybrid photocatalysts under visible light irradiation. MB was prepared with an initial concentration of 3.2 mg/L corresponding to 10^{-5} M (pH = 8). The hybrid photocatalysts were added into 30 mL of MB aqueous suspension with a concentration of 350 ppm. The photocatalytic removal of MB was carried out in a photoreactor with a 300 W light source (Osram UltraVitalux, 4.53% UV-A, 1% UV-B, 94.47% vis). The distance between the beakers and light source was kept constant at 20 cm for all specimens. Before irradiation, the solutions were kept in the dark medium for 10 min, to provide

equilibrium of adsorption/desorption. After that, the lamp was turned on to initiate the photocatalytic reactions. Along with all reactions, approximately 3 mL of MB aqueous solution was taken from each beaker at 30 min, 60 min, 90 min, 120 min, 180 min, and 240 min. Afterward, ejected samples measured with a UV spectrophotometer (Shimadzu UV 1240) device for absorption spectra of MB. All measurements were performed based on the characteristic absorption of MB peak at 664 nm.[51] The obtained absorbance values for each sample were converted to concentration values. TheBeer–Lambert law was used to examine the relationship between absorbance and concentration. The photocatalytic degradation efficiency was calculated according to the formula $[(C_0 - C)/C_0] \times 100$ (C_0, initial concentration; C, reaction concentration).[46] The efficiency of a photocatalytic reaction is very important issue for determination of any catalyst to be transferred into the application area.

RESULTS AND DISCUSSION

Structural Analysis

Fig. 2a shows the XRD patterns of the Gr, GO and rGO. The characteristic peak of Gr was obtained at 2θ of 26.44° with an interlayer spacing of 3.37 Å corresponding to the (002) lattice plane. This represents the crystalline nature of pristine Gr. In the XRD pattern of the GO, the characteristic peak due to the formation of oxygen functional groups in Gr layers shifted to 2θ of 12.14° indicating the expansion of the interlayer spacing to 7.8 Å. The increase in interlayer spacing can be attributed to the presence of oxygen functional groups which simplify the hydration and exfoliation of the graphene layer in the aqueous medium and oxidation of the Gr powder.[52–54] After the reduction of GO through N_2H_4, due to the removal of oxygen functional groups, the peak at 2θ of 12.14° disappeared and the splay peak between 2θ of 17- and 31° with a maximum intensity at 2θ of 25.54° was observed. The vanishing of the peak at 2θ of 12.14° is attributed to the disruption of regular stacking of the GO layers.[55]

Figure 2b shows the XRD patterns of TiO_2/rGO hybrid photocatalysts doped with various amounts of Ag. Diffraction peaks at 2θ of 25.27°, 37.88°, 48.22°, 53.97°, 54.96°, 62.8°, 69°, 70.1°, 75.3°, and 83.1° were indexed to (101), (004), (200), (105), (211), (204), (116), (220), (215), and (303) crystal planes of anatase TiO_2 (ICDD-21-1272), respectively.[50] Structural parameters and diffraction peaks are given in Table II. The XRD patterns of TiO_2/rGO hybrid photocatalysts show that it is completely in anatase phase with no detected diffraction pattern for the rGO. Therefore, it can be concluded that the addition of rGO and Ag developed no any new crystal planes nor changed the crystallographic orientation of TiO_2 due to the lower amount and relatively low diffraction intensity. Also, the disappearance of the

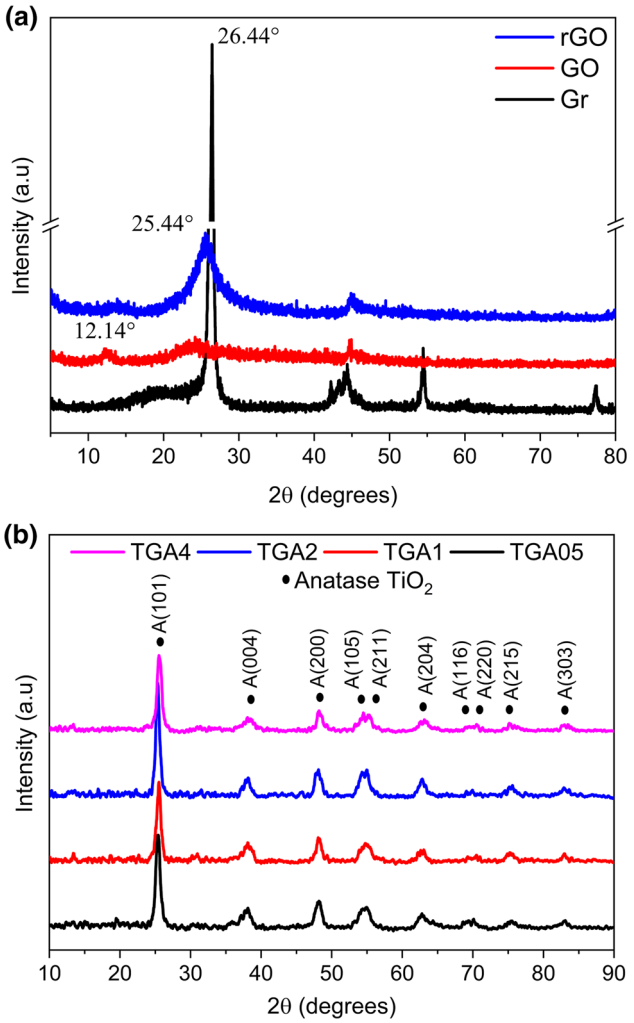

Fig 2. XRD patterns of (a) Gr, GO and rGO, (b) TGA05, TGA1, TGA2, TGA4.

diffraction patterns of rGO can be attributed to their overlapping patterns with the anatase phase pattern at 2θ of 25.27°.

With the aid of the Debye–Scherrer (Eq. 1) and Williamson–Hall (Eq. 2) methods, the crystallite size of the TGA hybrid photocatalysts was determined using the intensities of the main peak at 2θ value of 25°.[56] The dislocation density of the hybrid photocatalysts was calculated using Eq. 3:

$$D = \frac{k\lambda}{\beta T \cos\theta} \tag{1}$$

$$\beta T \cos\theta = \frac{k\lambda}{D\cos\theta} + 4\varepsilon \sin\theta \tag{2}$$

$$\delta = \frac{1}{D^2} \tag{3}$$

where k = 0.94, λ is the wavelength of the radiation used, β_T is the full width at half maximum of the

Table II. Microstructural parameters for TGA samples

Composition	Unit cell			Debye–Scherrer method		Williamson–Hall method			
	a (Å)	c (Å)	V (Å^3)	Crystallite size (nm)	Strain (× 10^3)	Crystallite size (nm)	Strain (× 10^3)	δ × 10^{14} lines/m^2	2θ of (101) plane
TGA05	3.78	9.49	10.88	10.88	4.904	6.59	− 1.27	84.48	25.3
TGA1	3.79	9.47	11.15	11.15	2.590	6.58	− 2.32	80.44	25.27
TGA2	3.79	9.49	12.35	12.35	2.176	9.61	1.04	65.56	24.24
TGA4	3.79	9.48	10.71	10.71	2.324	6.61	0.18	87.18	25.27

peak in radians and θ is the Bragg diffraction angle, D is the effective crystallite size, ε is the effective value of microstrain, and δ length of dislocation per unit volume of the crystal. The crystallite size, strain and dislocation density values of the TGA hybrid photocatalysts are given in Table II.

Williamson–Hall plots represent a linear plot of $4\sin\theta$ versus $\beta_T\cos\theta$ for the TGA samples in Fig. 3. The positive slope indicates that the system is under tensile stress, while the negative slope indicates that the system is under compressive strain.[57] The calculated crystalline sizes and strain values of TGA samples according to the Williamson–Hall method were lower than those obtained according to the Debye–Scherrer equation. This difference was observed to be due to line broadening and instrumental errors.[58]

In the literature, Ag doping has an effect on the crystallization of TiO_2.[59] Accordingly, in some cases crystallization increases with Ag doping, but in other cases they are reduced or not affected. The presence of Ag in the structure of the TiO_2/rGO hybrid composite causes a strain on the lattice and thus increases or decreases the crystallite size.[60,61]

It is known that dislocations are linear lattice defects seen in crystalline materials. The dislocation densities of TGA05, TGA1 and TGA4 were nearly identical; however, it was a very low value for TGA2 compared to the others. Some studies in the literature have shown that the crystallization is better with the decrease of defects, which means an increase in the crystallite size.[56, 62–64] The obtained results from structural analysis in this study are in a good agreement with the results in the literature.[65–67]

Morphological Analysis

Two-dimensional rGO sheets with curved shape can be seen in the SEM image of Fig. 4a. In Fig. 4b, the TiO_2 particles synthesized by sol–gel method appear to be nano-sized. It is also observed that there is some agglomeration. Figure 4c shows the TiO_2/rGO structure consisting of TiO_2 nanoparticles adhered to the rGO surface. Also present in the structure are rGO and TiO_2 which have not interacted with each other. TiO_2 nanoparticles, rGO layers, and TiO_2/rGO composite structures are shown in Fig. 4c. It is observed from Fig. 4d that there is no significant effect on the microstructure, which is attributed to a low doping concentration ratio of Ag, with Ag doping into the TiO_2/rGO hybrid composite structure.

Chemical Bonding and Phase Constitution

XPS analysis was carried out to determine the chemical states and composition of all samples. Figure 5 shows the XPS high-resolution spectra of all TGA samples in the region of Ag3d (a), O1s (b), Ti2p (c), and C1s (d), respectively. The Ag3d photoelectron peaks usually have two special peaks, which depend on $Ag3d_{5/2}$ and $Ag3d3_{3/2}$ transitions. The $Ag3d_{5/2}$ and $Ag3d_{3/2}$ peaks for metallic silver have maximum intensity at 368.8 eV and 374.7 eV, respectively.[68–70] Moreover, splitting of 5.9 eV between two peaks is associated with the production of metallic Ag in the TiO_2/rGO composites by the sol–gel process. The strong interaction between the Ag and defective regions of TiO_2 and the induced electrons transferred from TiO_2 to Ag were observed to show a low-level shift in the binding energy. The XPS spectra of O1s includes of two peaks at a binding energy of 530.9 and 533.08 based on the Ti–O bonds which are coherent with the binding energy of O^{-2} in the TiO_2 lattice and separated oxygen or hydroxyl (H–O) and/or carboxyl groups (C–O) in the composites, respectively.[68–70] In high-resolution XPS spectra of Ti2p, $Ti2p_{3/2}$ and $Ti2p_{1/2}$ peaks have been observed at binding energies of 459.6 eV and 465.4 eV, respectively, which is consistent with the value of Ti^{+4} in the TiO_2 lattice.[68–70] In the XPS narrow scan spectra of C1s, the main peak was observed around 285.8 eV, which corresponds to the extrinsic elemental carbon adsorbed on the surface of the sample (C–C) and intrinsic carbon which comes from Ti–O–C/C=C bonds.[70] The peak at 289.7 eV belongs to Ti–O–C=O showing the chemical bonding Ti with the carbon which stays on the surface of rGO.[70] According to these results, it was seen that Ti, oxygen vacancy states and impurities affected the doping level of Ag in the structure.

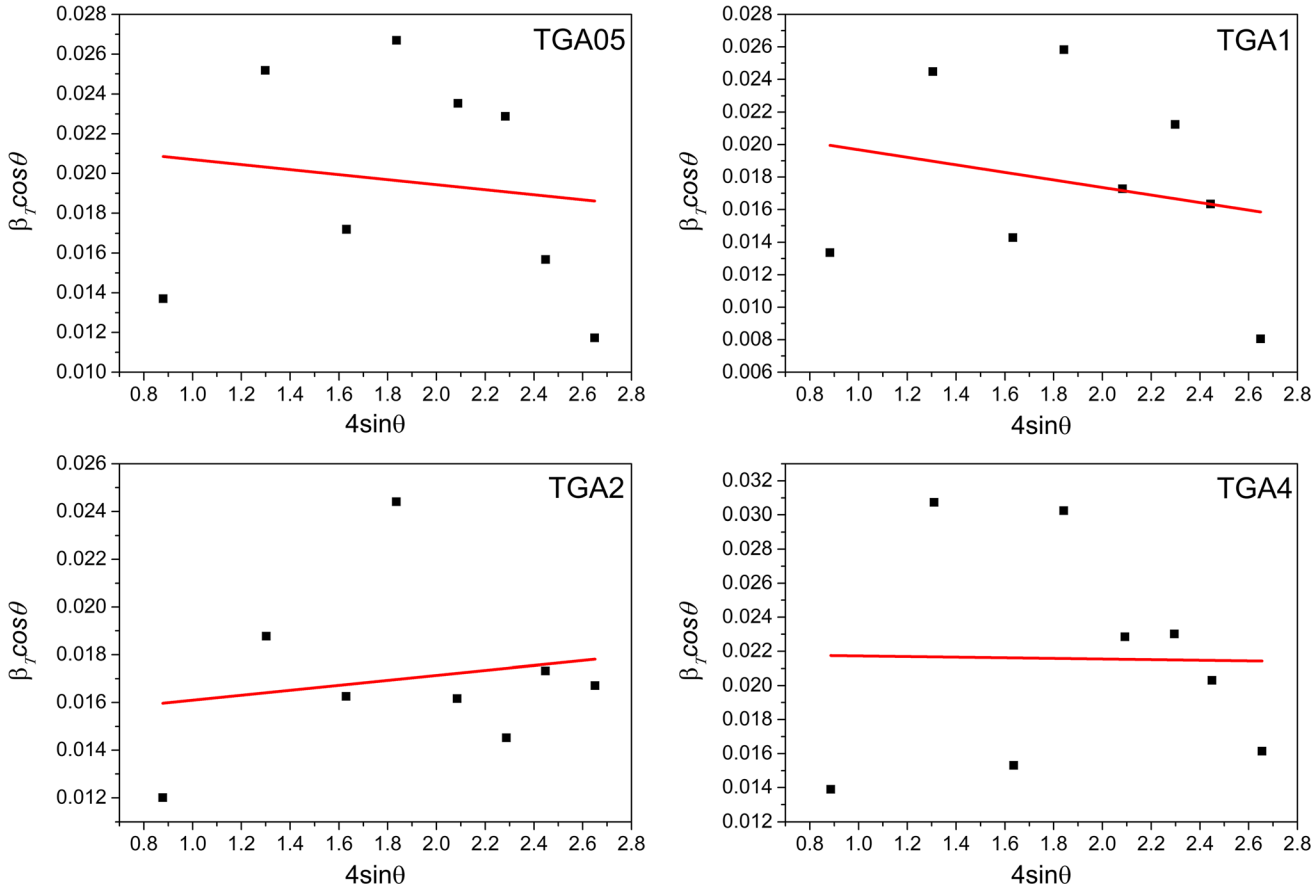

Fig 3. Williamson–Hall plots of TGA samples.

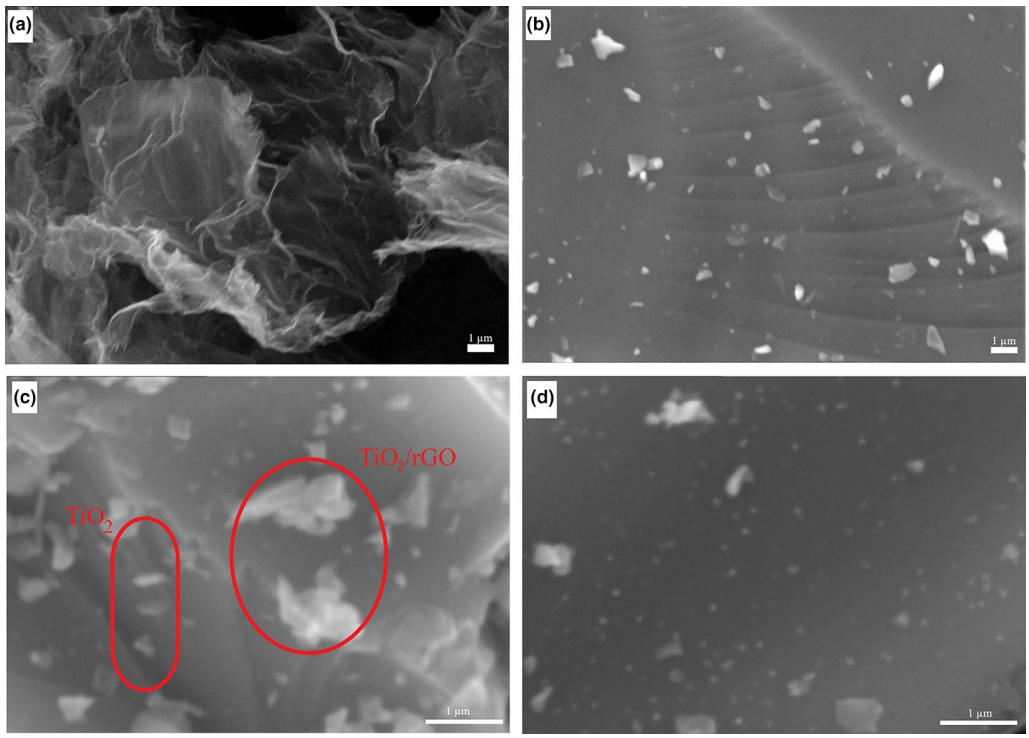

Fig 4. SEM images of (a) rGO, (b) TiO_2, (c) TiO_2/rGO, (d) TGA1.

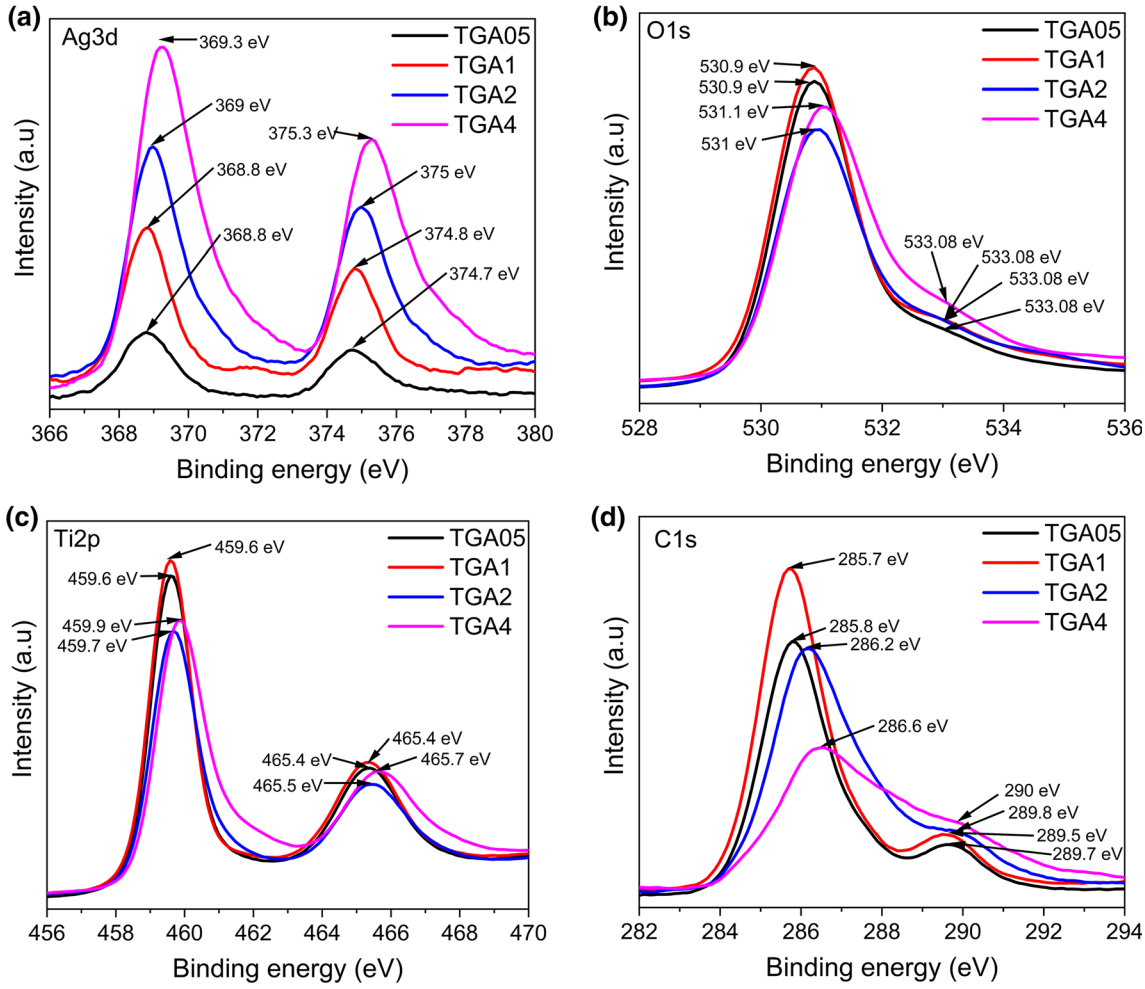

Fig 5. XPS patterns of (a) Ag3d, (b) O1s, (c) Ti2p, (d) C1s.

Optical Properties

The light reflectance property of TGA samples was measured with DRS. The band gap energy values were determined based on Kubelka–Munk transformation $(F(R)h\nu)^2$, where R is the intensity of reflection and $h\nu$ is the photon energy. In order to determine the direct band gap of the TGA samples, tangent lines are drawn until they intersects the hv axis from the linear area of the curve. The reflectance spectra and plot of $(F(R)h\nu)^2$ versus photon energy ($h\nu$) are demonstrated in Fig. 6a and b, respectively. The obtained band gap values are listed in Table III. As the Ag doping ratio increases from 0.5 wt.% to 4 wt.%, the band gap values of the samples decreases from 3.18 to 3.11.

PL spectroscopy is a well-known technique for measuring, understanding and proving the recombination rate of electron–hole pairs. As is known, the intensity of PL spectra is directly related to the recombination of electron–hole pairs.[71] The higher PL intensity indicates the increase in recombination rate which is not desired for photocatalytic studies.[72] If dopant ions such as Ag, Mo, Ce, rGO and defect areas such as Ti, Zn, Fe are present as trapping agents, the recombination rate and PL intensity decrease, thus photocatalytic activity, increase.[73]

The PL spectra of all produced samples are shown in Fig. 7. The TGA samples show two main emission peaks at 464 and 531 nm. It can be clearly seen that the TGA1 sample has the lowest PL intensity at 531 nm. The decrement of PL intensity at 531 nm demonstrated the decreasing recombination rate of excited electron–hole pairs. PL spectra of the samples show the presence of vacancies and/or interstitials which have a prominent effect on extending the lifetime of excited electrons. This was due to the migration of excited electrons to Ag clusters and/or seperation sites in the multiple phase structures of Ag@TiO_2/rGO hybrid photocatalysts in good agreement with the literature.[74, 75] It can be clearly said from the results that doping of Ag has a significant influence on the absorption of light. Considering these results, the TGA1 sample is expected to have the highest photocatalytic activity.

Photocatalytic Activity

The photocatalytic performances of TGA hybrid photocatalysts were obtained for the degradation of MB (10^{-5} M) aqueous solution by taking absorbance data at certain time intervals. With the photocatalytic effect, photocatalysts decolorize the MB aqueous solution over time under UV-visible light irradiation. Surface area, crystallinity, phase composition, and crystal orientation have an effect on the photocatalytic performances.[76–81] Figure 8a shows the relative concentration rate of MB by TGA hybrid photocatalysts which have Ag content from 0.5 wt.% to 4 wt.% during 240 min. From the absorbance values of the characteristic peak of the MB at 664 nm, concentration data were obtained using the Lambert–Beer law (Eq. 4)[50, 56] and are shown in Fig. 8b. The photocatalytic parameters of all samples are given in Table III.

$$\ln \frac{C_0}{C} = kt \tag{4}$$

where C_0, C and k correspond to the initial concentration of MB, concentration at certain time and kinetic rate constant, respectively. The slope of the line obtained from Fig. 8b gives the k value. The obtained k values indicate that the most enhancement of photocatalytic degradation of MB is achieved with 98.4% degradation efficiency by the TGA1 hybrid photocatalyst.

The degradation efficiencies of the MB, which had an initial absorbance value of 0.683 at 664 nm, were calculated for different samples and are indicated in Table III. Degradation efficiencies of MB by different hybrid photocatalysts under UV irradiation were also given as a bar chart in Fig. 9. As can be seen from the Fig. 9, the TGA1 hybrid photocatalyst has the best photocatalytic performance with a degradation efficiency of 98.4% in 240 min. As another observation, photocatalytic performance

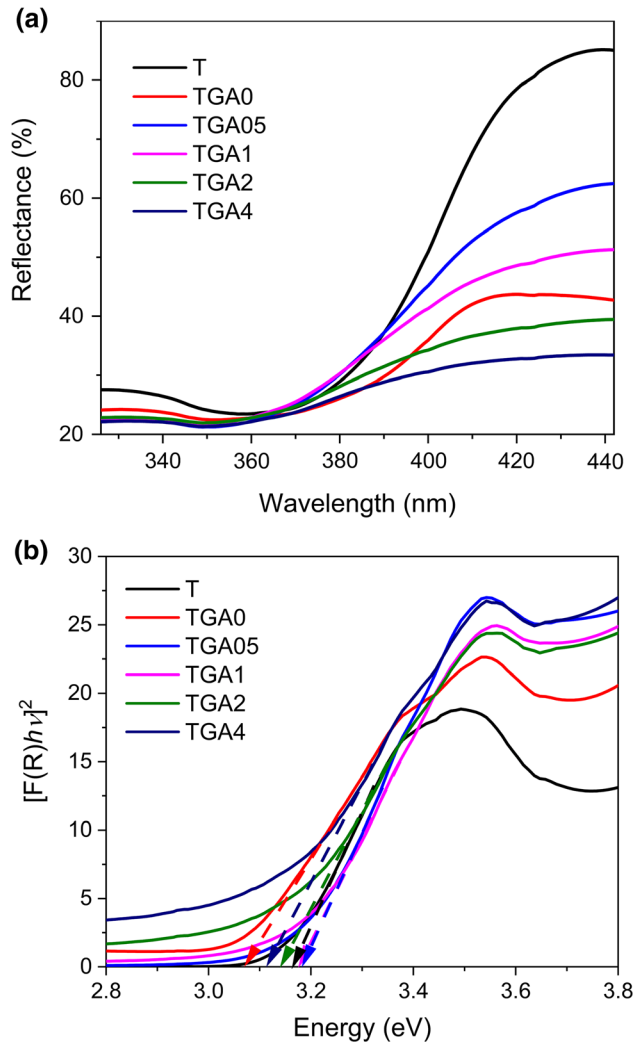

Fig 6. (a) Reflectance spectra of the TGA samples, (b) Plot of $(F(R)h\nu)^2$ versus photon energy ($h\nu$) TGA samples.

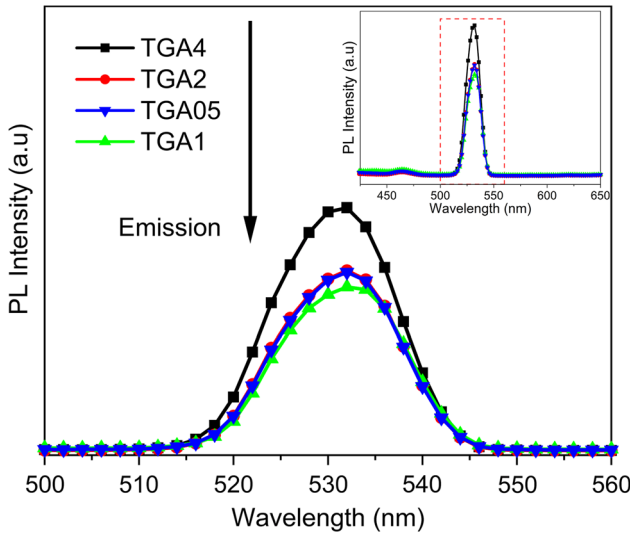

Fig 7. PL spectra of TGA samples.

Table III. Photocatalytic parameters and band gap values of TGA hybrid photocatalysts

Sample	TGA05	TGA1	TGA2	TGA4
Degradation efficiency (%)	94.7	98.4	93.0	84.0
Kinetic rate constant (k) (10^{-3} min^{-1})	12.32	17.2	11.06	7.65
R^2	0.9997	0.9945	0.9992	0.9995
Band gap	3.18	3.17	3.14	3.11

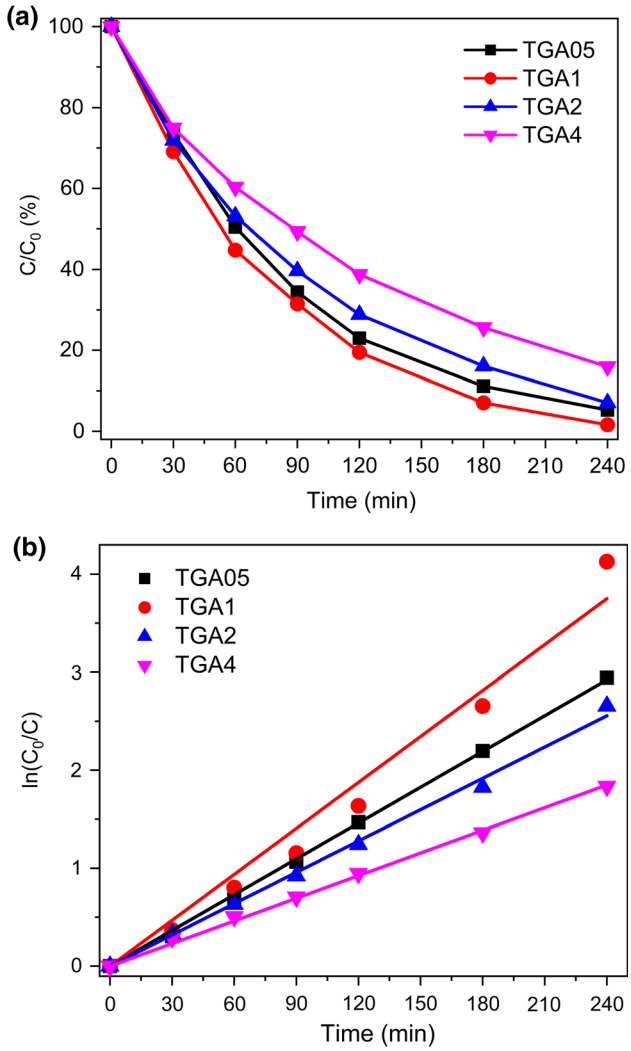

Fig 8. (a) Photocatalytic degradation of MB; (b) Photocatalytic kinetics of the TGA hybrid photocatalysts.

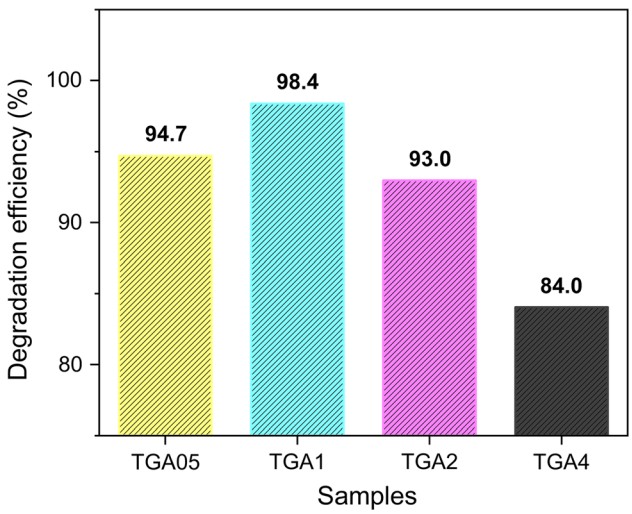

Fig 9. Degradation efficiencies of MB by TGA hybrid photocatalysts under UV light irradiation.

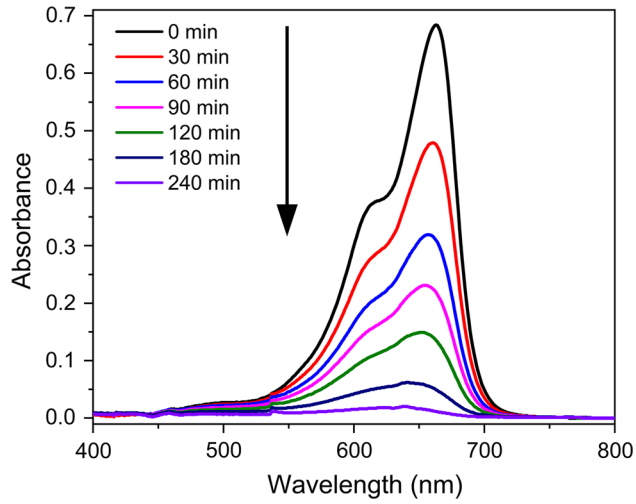

Fig 10. UV absorption spectra of the MB dye measured after the photocatalysis process.

increases with the increasing of Ag concentration from 0.5 wt.% to 1 wt.%, reaches a maximum at 1 wt.% (TGA1), and then decreases with the further increase of Ag concentration.

It can be clearly seen from Figs. 8 and 9 that the best photocatalytic degradation of MB is obtained in the presence of TGA1 hybrid photocatalyst. The absorption spectra of MB for TGA1 sample gradually decreased with increasing UV illumination time and shown in Fig. 10. The absorbance value of MB was decreased from 0.683 to 0.011 at 664 nm in the presence of the TGA1 sample under UV light exposure for 240 min.

The photocatalytic mechanism of TGA hybrid photocatalysts is shown in Fig. 11. The enhancement of the photocatalytic effect in this mechanism can be attributed to the synergistic interaction between Ag, Ti, and rGO. When the light is stimulated, the transition of the electrons in the valence band of the TiO_2 to the conduction band is provided. Thus, in the valence band, holes (h^+) are formed, while electrons (e^-) pass through the conduction band. As normally TiO_2 is stimulated by light, electron–hole pairs are quickly recombined. However, once the rGO is added to the structure, the electrons that pass through the conduction band tend to switch over to the rGO layers, which are very good at electrical conduction, rather than returning to the holes in the valence band. With the presence of rGO, the Ti–O–C and Ti–O–C=O bonds help to cause shifting of the TiO_2 absorption band edge.[82, 83] Thanks to this phenomenon, photogenerated electrons absorb low-energy photons and rGO also serves as an electron acceptor for TiO_2 conductive band electrons.[82, 84] Because of the π–π conjunction between MB and the aromatic region of rGO, absorptivity of the catalyst increases. The electrons trapped by rGO can also initiate the decomposition of MB directly.[82] Since the Fermi

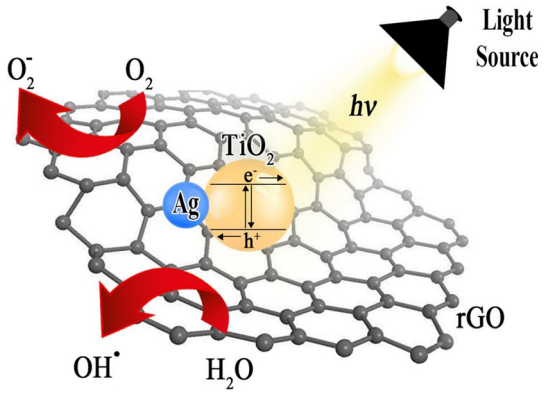

Fig 11. The photocatalytic mechanism of TGA hybrid photocatalysts.

level of TiO_2 is higher than Ag nanoparticles, when there is contact, a Schottky junction occurs between them and thus the transfer of electrons from Ag to TiO_2 is blocked. However, photoinduced electrons from Ag nanoparticles in TGA hybrid photocatalysts can overcome the Schottky barrier and pass to the conduction band of the TiO_2.[85–87] With the Ag doping into the TiO_2/rGO structure result in a significant increase of MB degradation which is due to physicochemical properties of the final product. However, overloading of Ag dopant content in TiO_2/rGO causes less photocatalytic performance. This may be attributed to the fact that Ag precipitates in the TiO_2 crystal matrix and/or is deposited on grain boundaries.[82] In addition, the increased amount of Ag acts as a barrier between the TiO_2/rGO photocatalysts, resulting in a relatively reduced concentration of charge carriers formed by the UV light irradiation.

Oxygen molecules (O_2) creates superoxide radical anions ($\cdot O^{2-}$) form with O_2 which formed from TiO_2/rGO composite by inducing by UV light source. These $\cdot O^{2-}$ anions degrade the MB into green compounds such as carbon dioxide (CO_2) and water (H_2O). The reactions that occur during the degradation of MB under the UV light source are as follows:

$$TiO_2 + h\upsilon \rightarrow TiO_2(h^+ + e^-) \quad (5)$$

$$rGO + e^- \rightarrow rGO(e^-) \quad (6)$$

$$Ag + e^- \rightarrow Ag(e^-) \quad (7)$$

$$O_2 + e^- \rightarrow \cdot O_2^- \quad (8)$$

$$H_2O + h^+ \rightarrow \cdot OH + H^+ \quad (9)$$

$$h^+ + \cdot O_2^- + \cdot OH + MB \rightarrow CO_2 + H_2O \quad (10)$$

CONCLUSION

Ag-doped TiO_2/rGO hybrid photocatalysts with high efficiency have been produced successfully by sol–gel method. It has been shown that the addition of Ag into the TiO_2/rGO structure greatly enhanced the photocatalytic activity of the composite catalyst. This enhancement might be related to the synergistic effects of wide range light absorption, higher charge separation, lower charge recombination, and enhanced absorptivity. The increase of the absorptivity of the catalyst is attributed to the structure of 2D planar surface of rGO and higher π–π interaction between TiO_2 and rGO. Ag and rGO have played an active role in the formation of high-performance photocatalyst composites. As a result of this study, it has been observed that Ag-doped TiO_2/rGO hybrid photocatalysts can be used very efficiently in removing organic pollutants.

REFERENCES

1. L. Yang, Y. Luo, L. Yang, S. Luo, X. Luo, W. Dai, T. Li, and Y. Luo, *J. Hazard. Mater.* 367, 550 (2019).
2. J. Fan, Z. Li, W. Zhou, Y. Miao, Y. Zhang, J. Hu, and G. Shao, *Appl. Surf. Sci.* 319, 75 (2014).
3. A. Miyoshi, S. Nishioka, and K. Maeda, *Chem. - A Eur. J.* 24, 18204 (2018).
4. C.H. Ao, and S.C. Lee, *Chem. Eng. Sci.* 60, 103 (2005).
5. A. Tereshchenko, R. Viter, I. Konup, V. Ivanitsa, S. Geveliuk, Y. Ishkov, and V. Smyntyna, in *Biophotonics—Riga 2013* (SPIE, 2013), p. 90320T.
6. X. Yan, Z. Wang, M. He, Z. Hou, T. Xia, G. Liu, and X. Chen, *Energy Technol.* 3, 801 (2015).
7. M. Ge, C. Cao, J. Huang, S. Li, Z. Chen, K.Q. Zhang, S.S. Al-Deyab, and Y. Lai, *J. Mater. Chem. A* 4, 6772 (2016).
8. K. Lee, H. Yoon, C. Ahn, J. Park, and S. Jeon, *Nanoscale* 11, 7025 (2019).
9. S. Sreeja and V. Shetty, *Sol. Energy* 157, 236 (2017).
10. E. Kowalska, H. Remita, C. Colbeau-Justin, J. Hupka, and J. Belloni, *J. Phys. Chem. C* 112, 1124 (2008).
11. V. Subramanian, E.E. Wolf, and P.V. Kamat, *J. Am. Chem. Soc.* 126, 4943 (2004).
12. L. Zhang, J.C. Yu, H.Y. Yip, Q. Li, K.W. Kwong, A.W. Xu, and P.K. Wong, *Langmuir* 19, 10372 (2003).
13. T. Ohno, M. Akiyoshi, T. Umebayashi, K. Asai, T. Mitsui, and M. Matsumura, *Appl. Catal. A Gen.* 265, 115 (2004).
14. R. Asahi, T. Morikawa, T. Ohwaki, K. Aoki, and Y. Taga, *Science (80-.)* 293, 269 (2001).
15. S. Sakthivel and H. Kisch, *Angew. Chemie Int. Ed.* 42, 4908 (2003).
16. Y. Z. Ma, J. Stenger, J. Zimmermann, S. L. Dexheimer, G. R. Fleming, S. M. Bachilo, R. E. Smalley, and R. B. Weisman, in *OSA Trends Opt. Photonics Ser.* (Optical Society of American (OSA), 2004), pp. 697–698.
17. S. Füldner, R. Mild, H.I. Siegmund, J.A. Schroeder, M. Gruber, and B. König, *Green Chem.* 12, 400 (2010).
18. J. Xu, W. Wang, S. Sun, and L. Wang, *Appl. Catal. B Environ.* 111–112, 126 (2012).
19. W. Cui, Y. Qi, L. Liu, D. Rana, J. Hu, and Y. Liang, *Prog. Nat. Sci. Mater. Int.* 22, 120 (2012).
20. W. Cui, D. Guo, L. Liu, J. Hu, D. Rana, and Y. Liang, *Catal. Commun.* 48, 55 (2014).
21. B. Ahmmad, Y. Kusumoto, S. Somekawa, and M. Ikeda, *Catal. Commun.* 9, 1410 (2008).
22. S. Battiston, M. Bolzan, S. Fiameni, R. Gerbasi, M. Meneghetti, E. Miorin, C. Mortalò, and C. Pagura, *Carbon N. Y.* 47, 1321 (2009).
23. H. Wang, X. Quan, H. Yu, and S. Chen, *Carbon N. Y.* 46, 1126 (2008).

24. J. Shi, G. Chen, G. Zeng, A. Chen, K. He, Z. Huang, L. Hu, J. Zeng, J. Wu, and W. Liu, *Ceram. Int.* 44, 7473 (2018).
25. Z. Song, T. Xu, M.L. Gordin, Y.B. Jiang, I.T. Bae, Q. Xiao, H. Zhan, J. Liu, and D. Wang, *Nano Lett.* 12, 2205 (2012).
26. C. Liu, L. Zhang, R. Liu, Z. Gao, X. Yang, Z. Tu, F. Yang, Z. Ye, L. Cui, C. Xu, and Y. Li, *J. Alloys Compd.* 656, 24 (2016).
27. B.A. Bhanvase, T.P. Shende, and S.H. Sonawane, *Environ. Technol. Rev.* 6, 1 (2017).
28. X. Niu, J. Yu, L. Wang, C. Fu, J. Wang, L. Wang, H. Zhao, and J. Yang, *Appl. Surf. Sci.* 413, 7 (2017).
29. W. Zhao, Z. Zhang, J. Zhang, H. Wu, L. Xi, and C. Ruan, *Mater. Lett.* 171, 182 (2016).
30. W. Dong, Y. Zhu, H. Huang, L. Jiang, H. Zhu, C. Li, B. Chen, Z. Shi, and G. Wang, *J. Mater. Chem. A* 1, 10030 (2013).
31. S. Anandan, T. Narasinga Rao, M. Sathish, D. Rangappa, I. Honma, and M. Miyauchi, *ACS Appl. Mater. Interfaces* 5, 207 (2013).
32. B. Jiang, C. Tian, Q. Pan, Z. Jiang, J.Q. Wang, W. Yan, and H. Fu, *J. Phys. Chem. C* 115, 23718 (2011).
33. S. Min, J. Hou, Y. Lei, X. Ma, and G. Lu, *Appl. Surf. Sci.* 396, 1375 (2017).
34. X. Li, R. Shen, S. Ma, and X. Chen, J. Xie, *Appl. Surf. Sci.* 430, 53 (2018).
35. A.A. Isari, A. Payan, M. Fattahi, S. Jorfi, and B. Kakavandi, *Appl. Surf. Sci.* 462, 549 (2018).
36. L. Cheng, Q. Xiang, Y. Liao, and H. Zhang, *Energy Environ. Sci.* 11, 1362 (2018).
37. C. Chen, Y. Zhang, J. Zeng, F. Zhang, K. Zhou, C.R. Bowen, and D. Zhang, *Appl. Surf. Sci.* 424, 170 (2017).
38. Q. Xiang, J. Yu, and M. Jaroniec, *Chem. Soc. Rev.* 41, 782 (2012).
39. Y. Xu, Y. Mo, J. Tian, P. Wang, H. Yu, and J. Yu, *Appl. Catal. B Environ.* 181, 810 (2016).
40. M. A. Syed, T. S. Muahammad, F. Muhammad, A. Sharjeel, and M. Isna, in *Key Eng. Mater.* (Trans Tech Publications Ltd, 2018), pp. 144–150.
41. Y. Liu, D. Zhang, Y. Shang, W. Zang, and M. Li, *RSC Adv.* 5, 104785 (2015).
42. Q. Xiang, J. Yu, and M. Jaroniec, *Nanoscale* 3, 3670 (2011).
43. W. Fan, X. Yu, H.C. Lu, H. Bai, C. Zhang, and W. Shi, *Appl. Catal. B Environ.* 181, 7 (2016).
44. P. K. Dubey, P. Tripathi, R. S. Tiwari, A. S. K. Sinha, and O. N. Srivastava, in *Int. J. Hydrogen Energy* (Elsevier Ltd, 2014), pp. 16282–16292.
45. A.L. Linsebigler, G. Lu, and J.T. Yates, *Chem. Rev.* 95, 735 (1995).
46. N.R. Khalid, E. Ahmed, M. Ahmad, N.A. Niaz, M. Ramzan, M. Shakil, T. Iqbal, and A. Majid, *Ceram. Int.* 42, 18257 (2016).
47. W. S. Hummers and R. E. Offeman, *J. Am. Chem. Soc.* (1958).
48. T. Luttrell, S. Halpegamage, J. Tao, A. Kramer, E. Sutter, and M. Batzill, *Sci. Rep.* 4, (2015).
49. J. Zhang, P. Zhou, J. Liu, and J. Yu, *Phys. Chem. Chem. Phys.* 16, 20382 (2014).
50. M. Yurddaşkal, U. Kartal, and E. C. Doluel, *J. Polytech.* 23, 249 (2020).
51. Y. Yang, E. Liu, H. Dai, L. Kang, H. Wu, J. Fan, X. Hu, and H. Liu, *Int. J. Hydrogen Energy* 39, 7664 (2014).
52. H. Al-Kandari, A.M. Abdullah, S. Al-Kandari, and A.M. Mohamed, *RSC Adv.* 5, 71988 (2015).
53. V. Loryuenyong, K. Totepvimarn, P. Eimburanapravat, W. Boonchompoo, and A. Buasri, *Adv. Mater. Sci. Eng.* 2013, e923403 (2013).
54. A.R. Siamaki, A.E.R.S. Khder, V. Abdelsayed, M.S. El-Shall, and B.F. Gupton, *J. Catal.* 279, 1 (2011).
55. Y. Chen, Y. Niu, T. Tian, J. Zhang, Y. Wang, Y. Li, and L.C. Qin, *Chem. Phys. Lett.* 677, 143 (2017).
56. S. Demirci, T. Dikici, M. Yurddaskal, S. Gultekin, M. Toparli, and E. Celik, *Appl. Surf. Sci.* 390, 591 (2016).
57. S. Çakar and M. Özacar, *J. Photochem. Photobiol. A Chem.* 346, 512 (2017).
58. K.M. Prabu and S. Perumal, *Int. J. Sci. Res. Sci. Eng. Technol.* 1, 299 (2015).
59. J. García-Serrano, E. Gómez-Hernández, M. Ocampo-Fernández, and U. Pal, *Curr. Appl. Phys.* 9, 1097 (2009).
60. M.B. Suwarnkar, R.S. Dhabbe, A.N. Kadam, and K.M. Garadkar, *Ceram. Int.* 40, 5489 (2014).
61. W. Sangchay and I. Technology, *Int. J. Eng. Res. Appl.* 2, 1593 (2012).
62. S. Demirci, M. Yurddaskal, T. Dikici, and C. Sarıoğlu, *J. Hazard. Mater.* 345, 27 (2018).
63. M.M. Obeid, S.J. Edrees, and M.M. Shukur, *Superlattices Microstruct.* 122, 124 (2018).
64. M.M. Obeid, H.R. Jappor, K. Al-Marzoki, I.A. Al-Hydary, S.J. Edrees, and M.M. Shukur, *RSC Adv.* 9, 33207 (2019).
65. P. Malliga, J. Pandiarajan, N. Prithivikumaran, and K. Neyvasagam, *IOSR J. Appl. Phys.* 6, 22 (2014).
66. V.V. Kondalkar, S.S. Mali, N.B. Pawar, R.M. Mane, S. Choudhury, C.K. Hong, P.S. Patil, S.R. Patil, P.N. Bhosale, and J.H. Kim, *Electrochim. Acta* 143, 89 (2014).
67. L.M. Santos, W.A. Machado, M.D. França, K.A. Borges, R.M. Paniago, A.O.T. Patrocinio, and A.E.H. Machado, *RSC Adv.* 5, 103752 (2015).
68. N. Lu, Y. Wang, S. Ning, W. Zhao, M. Qian, Y. Ma, J. Wang, L. Fan, J. Guan, and X. Yuan, (n.d.).
69. S. K. Md Saad, A. Ali Umar, M. I. Ali Umar, M. Tomitori, M. Y. Abd. Rahman, M. Mat Salleh, and M. Oyama, *ACS Omega* 3, 2579 (2018).
70. X. Wei, J. Cao, and F. Fang, *RSC Adv.* 8, 31822 (2018).
71. T.G. Ulusoy, A. Ghobadiac, and A.K. Okyay, *J. Mater. Chem. A* 2, 16867 (2014).
72. T. Ali, P. Tripathi, A. Azam, W. Raza, A. S. Ahmed, A. Ahmed, and M. Muneer, *Mater. Res. Express* 4, (2017).
73. J. Liqiang, Q. Yichun, W. Baiqi, L. Shudan, J. Baojiang, Y. Libin, F. Wei, F. Honggang, and S. Jiazhong, *Sol. Energy Mater. Sol. Cells* 90, 1773 (2006).
74. J. Yu, J. Xiong, B. Cheng, and S. Liu, *Appl. Catal. B Environ.* 60, 211 (2005).
75. S. Gayathri, M. Kottaisamy, and V. Ramakrishnan, *AIP Adv.* 5, 127219 (2015).
76. M. Yurddaskal, *J. Inorg. Organomet. Polym. Mater.* 29, 2214 (2019).
77. J. Ryu, D.S. Park, B.D. Hahn, J.J. Choi, W.H. Yoon, K.Y. Kim, and H.S. Yun, *Appl. Catal. B Environ.* 83, 1 (2008).
78. M. Inagaki, R. Nonaka, B. Tryba, and A.W. Morawski, *Chemosphere* 64, 437 (2006).
79. A. Brudnik, A. Gorzkowska-Sobaś, E. Pamuła, M. Radecka, and K. Zakrzewska, *J. Power Sources* 173, 774 (2007).
80. M. Toyoda, Y. Nanbu, Y. Nakazawa, M. Hirano, and M. Inagaki, *Appl. Catal. B Environ.* 49, 227 (2004).
81. H.G. Yang, C.H. Sun, S.Z. Qiao, J. Zou, G. Liu, S.C. Smith, H.M. Cheng, and G.Q. Lu, *Nature* 453, 638 (2008).
82. H. Khan, Z. Jiang, and D. Berk, *Sol. Energy* 162, 420 (2018).
83. Z.K. Zhang, D.Z. Guo, Y.J. Xing, and G.M. Zhang, *Appl. Surf. Sci.* 257, 4139 (2011).
84. G. Lui, J.Y. Liao, A. Duan, Z. Zhang, M. Fowler, and A. Yu, *J. Mater. Chem. A* 1, 12255 (2013).
85. E. Vasilaki, I. Georgaki, D. Vernardou, M. Vamvakaki, and N. Katsarakis, *Appl. Surf. Sci.* 353, 865 (2015).
86. S. Oros-Ruiz, R. Zanella, and B. Prado, *J. Hazard. Mater.* 263, 28 (2013).
87. P. Wang, B. Huang, Y. Dai, and M.H. Whangbo, *Phys. Chem. Chem. Phys.* 14, 9813 (2012).